Letter

X-ray diffraction study of phase transformation dynamics of Fe and Fe-Si alloys along the shock Hugoniot using an x-ray free electron laser

A. Krygier,[1,2,*] M. Harmand,[1] B. Albertazzi,[3] E. E. McBride,[4,5] K. Miyanishi,[6,7] D. Antonangeli,[1] Y. Inubushi,[7,8] R. Kodama,[6,9] M. Koenig,[3,9] T. Matsuoka,[10] G. Mogni,[1] F. Pietrucci,[1] A. M. Saitta,[1] T. Togashi,[7,8] Y. Umeda,[9,11] T. Vinci,[3] M. Yabashi,[7,8] T. Yabuuchi,[7,8] G. Fiquet,[1] and N. Ozaki[6,9]

[1]*Sorbonne Université, Muséum National d'Histoire Naturelle, UMR CNRS 7590, Institut de Minéralogie, de Physique des Matériaux, et de Cosmochimie (IMPMC), F-75005 Paris, France*

[2]*Lawrence Livermore National Laboratory, 7000 East Avenue, Livermore, California 94550, USA*

[3]*LULI, CNRS, CEA, Sorbonne Université, Ecole Polytechnique, Institut Polytechnique de Paris, F-91120 Palaiseau Cedex, France*

[4]*European XFEL GmbH, Holzkoppel 4, D-22869 Schenefeld, Germany*

[5]*SLAC National Accelerator Laboratory, 2575 Sand Hill Road, MS 19, Menlo Park, California 94025, USA*

[6]*Institute for Laser Engineering, Osaka University, Suita, Osaka 565-0871, Japan*

[7]*RIKEN Spring-8 Center, Sayo, Hyogo 679-5148, Japan*

[8]*Japan Synchrotron Radiation Research Institute, Sayo, Hyogo 679-5198, Japan*

[9]*Graduate School of Engineering, Osaka University, Suita, Osaka 565-0871, Japan*

[10]*Open and Transdisciplinary Research Initiatives, Osaka University, Suita, Osaka 565-0871, Japan*

[11]*Institute for Integrated Radiation and Nuclear Science, Kyoto University, Sennan, Osaka 590-0494, Japan*

(Received 22 October 2021; revised 13 May 2022; accepted 19 May 2022; published 7 June 2022)

The x-ray free electron laser (XFEL) enables probing a highly compressed material response at the subnanosecond timescale. We exploit the ultrafast XFEL pulse to combine reflection x-ray diffraction and laser-driven shock compression to perform a study of the phase transformation and stability in Fe and Fe-Si alloys. Our approach enables us to observe that solid-solid phase transformations occur in Fe and Fe-$Si_{8.5\,wt\,\%}$ in $\leqslant$130 ps at ∼130 GPa; no transformation is observed in Fe-$Si_{16\,wt\,\%}$ up to 110 GPa. Density functional theory calculations predict similar phase relations.

DOI: 10.1103/PhysRevB.105.L220102

I. INTRODUCTION

High-pressure and temperature properties of Fe [1–6] and Fe-Si alloys [7–12] are important due to their prominence in geophysics, planetary science, and wide industrial use [13]. Fe is the main component of the core of telluric planets and Si is a potentially significant core alloy component for Earth, Mercury, and many exoplanets [14], in particular when formed under reducing conditions. Si is also a commonly used alloy element in high-performance steels and advanced magnetic materials [15]. The addition of Si is suggested to stabilize cubic phases over a large pressure and temperature range [16–19], at the expense of the hexagonally close-packed (hcp) structure, the ϵ phase of pure Fe at high pressure. In Fe, the transformation from an ambient body-centered-cubic (bcc) to hcp phase is martensitic and thus a rapid transformation. Despite significant effort, much about these materials remains unknown.

X-ray diffraction (XRD) measurements of Fe-Si alloys compressed using diamond anvil cells (DACs) and laser heated DAC (LH-DAC) [12,16,17,19–22] show disagreement. Hirao *et al.* [20] report that Fe-$Si_{8.7\,wt\,\%}$ transforms from an ambient bcc phase to hcp over pressures ∼16–35 GPa while the cubic phase remains stable in Fe-$Si_{17.8\,wt\,\%}$ up to ∼124 GPa (300 K). Fischer *et al.* [17] report that Fe-$Si_{9\,wt\,\%}$ transforms from a cubic to hcp phase around 45 GPa/1400 K, and suggest a phase boundary at ∼20 GPa/1000 K, with a $B2$-hcp mixture at higher temperature, up to melting. Fischer *et al.* [16] report that Fe-$Si_{16\,wt\,\%}$ transforms from a cubic $B2$ or $D0_3$ phase to a mixed $B2$-hcp phase above 50 GPa/1000 K. Edmund *et al.* [19] investigated the Si concentration dependence of the bcc-hcp transformation pressure and find an increase of ∼11.5 GPa/wt % Si between ∼8 and 12 wt % at 300 K and that the cubic phase remains stable in Fe-$Si_{17wt\,\%}$ up to ∼65 GPa. Wicks *et al.* [18] explored phase relations in Fe, Fe-$Si_{7\,wt\,\%}$, and Fe-$Si_{15\,wt\,\%}$ phase relations up to 1300 GPa using ramp compression and nanosecond XRD. Unlike Fischer [17] and consistent with Edmund [19] they observe no phase transformation in Fe-$Si_{15\,wt\,\%}$, possibly due to the lower temperature or the short timescale preventing dissociation into Si-rich $B2$ and Si-poor hcp. Despite the numerous studies and strong dependence of mechanical properties on the crystalline structure [4,23–25], the phase diagrams of Fe-Si alloys remain uncertain.

While static compression with DAC is widely used in high-pressure experiments, there are some drawbacks. These include limits on pressure and temperature, diffuse contamination of carbon from the anvil [3,26], the formation of preferred crystallite orientations [27], and the frequent

*krygier1@llnl.gov

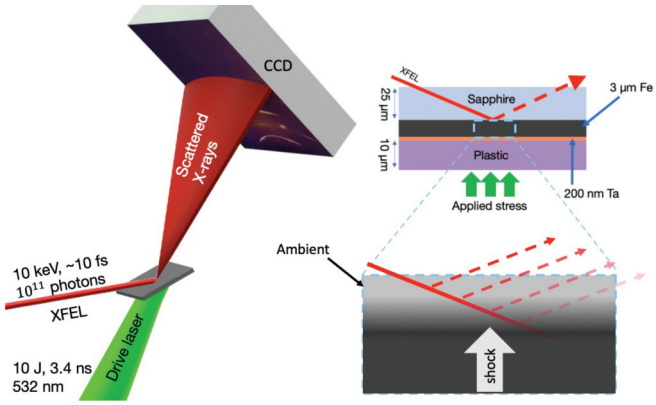

FIG. 1. Experimental configuration. The sample and probe geometry are detailed in the top right inset. The bottom right inset is a sketch highlighting the probe sensitivity to the traveling shock wave. The large incidence angle highly biases the probed volume to the rearmost 1 μm of the sample; this distance corresponds to the distance a shock wave in our conditions travels in ~130 ps.

need for a pressure scale [28,29]. Sample demixing can also occur from pressure- and temperature-induced solubility changes [30,31].

On the other hand, laser-driven dynamic compression can achieve very high pressures and temperatures and the sample composition is not likely to be impacted by diffusion due to the timescale. However, the x-ray sources typically available at laser-driven dynamic compression facilities are uncollimated and of nanosecond duration [32]. High-power lasers coupled to femtosecond XFEL sources now produce very high quality XRD of dynamically compressed samples [33–38].

In laser-driven dynamic compression, an expanding plasma drives a pressure wave into the sample, creating ~1–10 ns duration high-pressure states at strain rates up to $\sim 10^9$ s^{-1}. Though the initial strain is uniaxial, the sample rapidly approaches hydrostaticity through plasticity, phase transformation, or twinning [39], etc. A benefit of this approach is precise knowledge of the *in situ* sample composition, however, an interpretation of the results can be complicated by kinetic effects [1,5,40,41]. Smith *et al.* [5] and Amadou *et al.* [41] inferred that the bcc-hcp transformation occurs on the ~1 ns timescale in pure Fe and find a higher transformation onset stress than in static compression; kinetics in nonmetals can occur on longer timescales [33,42]. Recent measurements also report phase transformation boundary lowering in dynamic compression [36,37].

II. RESULTS

We use the ~10 fs x-ray pulse at the Spring-8 Angstrom Compact Free Electron Laser [43–45] (SACLA) facility to determine the crystal structure in compressed Fe, Fe-$Si_{8.5\,wt\,\%}$, and Fe-$Si_{16\,wt\,\%}$. Every experiment uses the same laser pulse shape and general sample design. The Paylene-N ablator is coated directly onto the Fe or Fe-Si layer (see Fig. 1), ensuring the shock state is not altered by reverberations from glue layers. The pulse duration, sample design, and geometry allow us to observe a rapid onset of the hcp phase in Fe and Fe-$Si_{8.5\,wt\,\%}$ during the initial shock and no structural transformation in Fe-$Si_{16\,wt\,\%}$ during the initial shock or on release, in disagreement with some early static measurements [16,17].

Figures 2(a) and 2(b) show raw XRD images from ambient and compressed Fe, respectively. The highly textured (preferred crystallite orientation) Fe samples produce azimuthally narrow XRD spots, which prevents the observation of some reflections, but enables exploitation of the known bcc-hcp orientation relationship [2,46]. Our analysis uses the textural similarity between the ambient and high-pressure diffraction. The high-pressure bcc {110} and {211} reflections in Fig. 2(b) have the same pattern as their ambient counterparts in Fig. 2(a) and correspond to the same bcc lattice parameter to within ~1%. We identify the hcp {002} reflection [Fig. 2(b), red] by combining knowledge of the initial bcc texture and *a priori* knowledge of the parent-child orientation relationship where the atoms comprising the bcc {110} plane become the hcp {002} plane, maintaining their initial orientation. This relationship, combined with their similar d spacings for our pressure, produces similar azimuthal bcc {110} and hcp {002} diffraction patterns.

Figure 3 shows integrated XRD patterns of ambient (dashed green line) and *in situ* high-pressure (solid purple line) Fe [Fig. 3(a)], Fe-$Si_{8.5\,wt\,\%}$ [Fig. 3(b)], and Fe-$Si_{16\,wt\,\%}$ [Fig. 3(c)]. The phase and corresponding reflection plane are labeled. Fe and Fe-$Si_{8.5\,wt\,\%}$ patterns include reflections from a ~100-nm Au deposition to aid sample alignment (see Supplemental Material [47]). Across our data, the shock rise time is 0.5 ± 0.1 ns, which combined with the directly measured strain gives a strain rate of $\dot{\epsilon} = (V_0 - V)/V_0)/\Delta t = 5.9 \times 10^8$ s^{-1}, below the extrapolated value from Swegle-Grady [48] for our pressures.

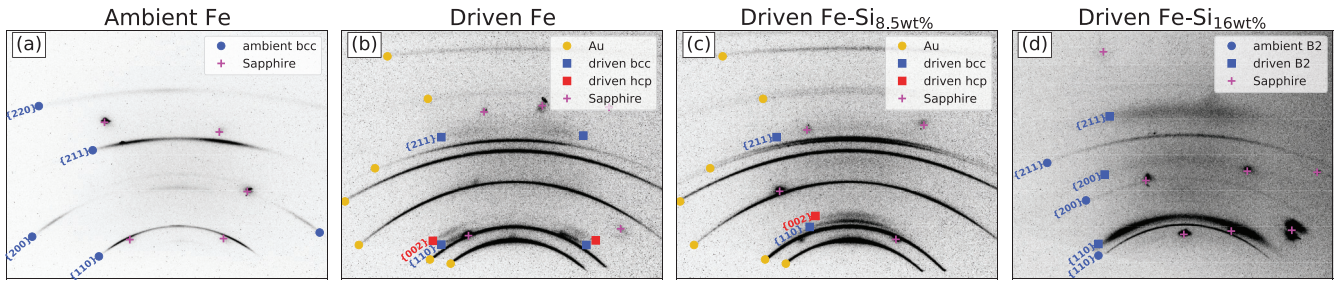

FIG. 2. Raw diffraction images of (a) ambient Fe, (b) driven Fe, (c) driven Fe-$Si_{8.5\,wt\,\%}$, and (d) driven Fe-$Si_{16\,wt\,\%}$. Circles (squares) indicate ambient (compressed) reflections. Gold circles indicate Au; pink pluses indicate sapphire. Blue and red markers indicate cubic (bcc/$B2$) and hcp phase reflections, respectively.

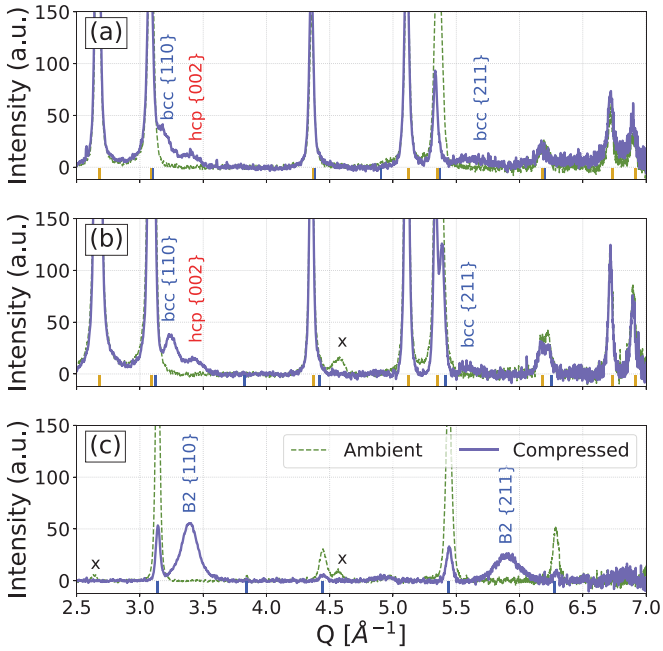

FIG. 3. Diffraction patterns of (a) shocked Fe, (b) Fe-$Si_{8.5\,wt\%}$, and (c) Fe-$Si_{16\,wt\%}$. Green (purple) curves denote ambient (compressed) samples. Gold (blue) ticks mark Au (ambient sample) reflections. Black × symbols indicate sample holder reflections; sapphire reflections are masked.

The Fe-$Si_{8.5\,wt\%}$ samples [XRD image in Fig. 2(c)] are textured differently than Fe, but the implied lattice parameter from the bcc {110} and {211} reflections [Fig. 3(b)] agree similarly, so we interpret the three reflections in the same way.

The Fe-$Si_{16\,wt\%}$ samples form the $B2$ structure at ambient conditions. Fischer *et al.* [16] report a $D0_3$ structure at ambient conditions in similar samples, however, $D0_3$ and $B2$ are structurally alike with $D0_3$ producing several additional weak reflections that might be below the detection threshold. Furthermore, physical vapor deposition synthesis at relatively low temperature does not favor Si ordering [15,19]. The data in Fig. 3 were collected during the initial shock. We therefore expected to see a $B2$ + hcp mixture in our conditions.

III. DISCUSSION

We neither find evidence of a structural phase transformation to the hcp structure reported by Fischer, nor other possible Fe-Si structures [49–51]. This includes measurements made during the initial shock over a range of pressures (∼10–110 GPa) and after releasing into the sapphire window. The disappearance of weaker reflections at high pressure is due to the background and noise generated by the ablation plasma, but does not invalidate our conclusions: We cannot distinguish bcc from $B2$ or $D0_3$ (references to $B2$ phase observation have this caveat throughout) but we can clearly discard the presence of a hcp phase. Wave profile measurements of shock- and ramp-compressed Fe report kinetics associated with the bcc-hcp transformation [1,5,40,41] and simulations of shocked Fe predict an elastic-plastic-transformation process [52–54]. Nevertheless, direct crystal structure measurements remain critical as the association between wave profile features and phase transformation must otherwise be assumed, which has been shown to be problematic in some materials [36].

Measuring x-ray diffraction with an XFEL and thin samples provides a nearly instantaneous snapshot of the crystallographic state—the ∼10 fs x-ray pulse and its time of flight across the sample are very short compared to hydrodynamic timescales. A 100 GPa shock in Fe has a shock velocity of ∼7000 m/s, meaning that the shock travels only ∼0.7 Å during the x-ray pulse, less than the inner-atomic distance. The time of flight of the x-ray pulse in our sample is also very short. At 70° incidence, it takes only ∼30 fs to transit the ∼3-μm-thick sample. During this time, the same 100 GPa shock travels only 2 Å, which is approximately the inner-atomic distance in Fe in a 100 GPa shock. This is a clear advantage over synchrotron and laser-driven x-ray sources which have durations of 0.1–1 ns.

In our geometry, x rays that contribute to the measured diffraction signal are incident on the rear surface and then reflected back through the same surface (see Fig. 3). This means that the path length through the sample rapidly increases with scattering depth and deeper parts of the sample contribute less signal due to stronger attenuation. This is different than the more common transmission geometry [37,38] where attenuation is more uniform with scattering depth. The reflection geometry therefore provides a comparatively strong rear-surface sensitivity. For example, the total path length in Fe of an x ray that diffracts from the ambient bcc {110} plane at a depth of 1 μm has a path length of ∼7 μm, similar to the attenuation length of 10.1-keV x rays. Considering only attenuation in Fe, 64% of detected x rays are scattered from the rearmost 1 μm of the sample. It would be possible to tune this sensitivity in most materials by selecting an appropriate x-ray probe energy.

We exploit these factors to record x-ray diffraction of the leading edge of the shock. On some experiments, the x-ray probe is timed before the shock breaks out of the sample. In these cases, both ambient and compressed states contribute to the signal, the former confirming the position of the shock in the sample and the latter corresponding to the leading edge of the shock wave (bottom right inset in Fig. 3). Again, considering only x-ray attenuation, this implies that any measured diffraction coming from the compressed sample is preferentially sensitive to the leading edge of the shock. In our conditions, a shock in Fe travels 1 μm in ∼130 ps, meaning that the signal from compressed Fe corresponds to the evolution of the shock on that timescale.

The simultaneous observation of compressed bcc and hcp phases is consistent with the transient compression dynamics described by Kadau [52–54]. The observation of the hcp phase in the leading edge of the shock effectively sets an upper bound of ∼130 ps on the bcc-hcp phase transformation onset in Fe and Fe-$Si_{8.5\,wt\%}$ under these conditions. This time resolution also allows us to confirm the inconsistency in the various phase diagrams proposed for Fe-$Si_{16\,wt\%}$ [17–19] and to propose a possible explanation for this disagreement below.

The d spacing of the transient, compressed Fe bcc phase corresponds to a hydrostatic pressure of 19.1 ± 6.6 GPa (SESAME 2150), though the conditions inside the shock front are not at equilibrium and our data are not sensitive to possible structural anisotropy associated with an elastic wave or

strength. The {002} hcp d spacing corresponds to a hydrostatic pressure of 128 ± 35 GPa. The pressure of the final state is well above the expected hcp onset stress determined by Smith *et al.* ($\sigma_{\alpha\to\epsilon} = 1.15 \times \dot{\epsilon}^{0.18}$) that evaluates to 44 GPa in our conditions, and so we would expect to observe hcp. The nature and dynamics of the initial compression remains an open and interesting question for future, tailored dynamic compression studies.

Hwang *et al.* [55] have also investigated shocked Fe on subnanosecond timescales, however, their results are difficult to interpret. Their calculated strain rate is significantly higher than expected for their shock pressures [48] and they report a significantly larger Hugoniot elastic limit (HEL) than previously observed [40], though how the HEL is identified is not clear. Temporal and spatial gradients may be important due to the very short pulse length (∼140 ps) and small laser focus (40 μm full width at half maximum Gaussian focus vs 20 μm XFEL probe area). How these effects impact the sampled hydrodynamic state is not easily discerned by argument and not addressed with measurements or multidimensional hydrodynamics simulations. Unlike Hwang *et al.*, we do not observe multiple features associated with compressed bcc, which may be due to the higher pressure in our Fe experiments and/or lower susceptibility to gradients.

Our results highlight the importance of investigating phase transformation dynamics in compression experiments before applying the results to constrain phase diagrams. They also highlight the advantage of using textured samples [39,56,57] for this purpose, and could be especially useful for identifying phase transformation orientation relationships and kinetics. Performing this experiment with a powder sample could hypothetically lead to incorrectly identifying the driven bcc {110} reflection as the hcp {100} plane. This would incorrectly yield a c/a ratio of 1.64 for the hcp phase, which is significantly higher than observed in either dynamic [58] or static [59] experiments, and could have misleading geophysical implications [60–62].

The reflections observed during the initial shock in Fe-$Si_{8.5\ wt\%}$ are similar to Fe, suggesting a similar interpretation and underlying phenomena. The transient bcc {110} and {211} d spacings correspond to 38 GPa hydrostatic pressure; the high-pressure hcp {002} corresponds to 132 ± 26 GPa pressure (using Hirao *et al.* [20]). We make no thermal corrections since the Hirao data agree well with the Fe-$Si_{6.9\ wt\%}$ shock Hugoniot data from Marsh *et al.* [63] (Fig. 4); measurements of Fe-$Si_{5\ wt\%}$ at slightly lower pressure [14] suggest the thermal pressure is ∼15 GPa for our conditions, similar to that found by Fischer *et al.* in Fe-$Si_{16\ wt\%}$ and less than our error bars. The inferred bcc pressure is consistent with our calculations for the transformation pressure described below. Given the rapid onset, this transformation in Fe-$Si_{8.5\ wt\%}$ is likely a nondiffusive process such as Fe's martensitic bcc-hcp phase transformation.

Conversely, we do not observe a phase transformation in Fe-$Si_{16\ wt\%}$. This disagrees with Fischer *et al.* [16], but agrees with Edmund *et al.* [19] at room temperature and ramp compression data from Wicks *et al.* [18] at moderate temperature.

Finally, we performed 0-K structural prediction calculations using density functional theory (DFT). Predicted phases between 0 and 120 GPa for Fe-$Si_{9.1\ wt\%}$ ($Fe_{10}Si_2$) and Fe-$Si_{16.7\ wt\%}$ ($Fe_{10}Si_4$ or Fe_5Si_2) were calculated by estimating the relative enthalpy of the main phases at the generalized gradient approximation (GGA)-Perdew-Burke-Ernzerhof (PBE) approximation level [65] for the exchange-correlation energy functional. These concentrations approximate the experimental conditions while managing calculation size. Nonmagnetic $B2$ and hcp phases use the larger $Fe_{10}Si_4$ cell; ferromagnetic $D0_3$ uses the smaller Fe_5Si_2 cell due to the heavier computational cost of magnetic calculations. Magnetic effects are implemented using a standard collinear spin-polarization model. Crystal structure predictions were made with the *Ab Initio* Random Structure Search [66] code coupled with efficiency enhancements described in the Supplemental Material [47] and detailed separately [67].

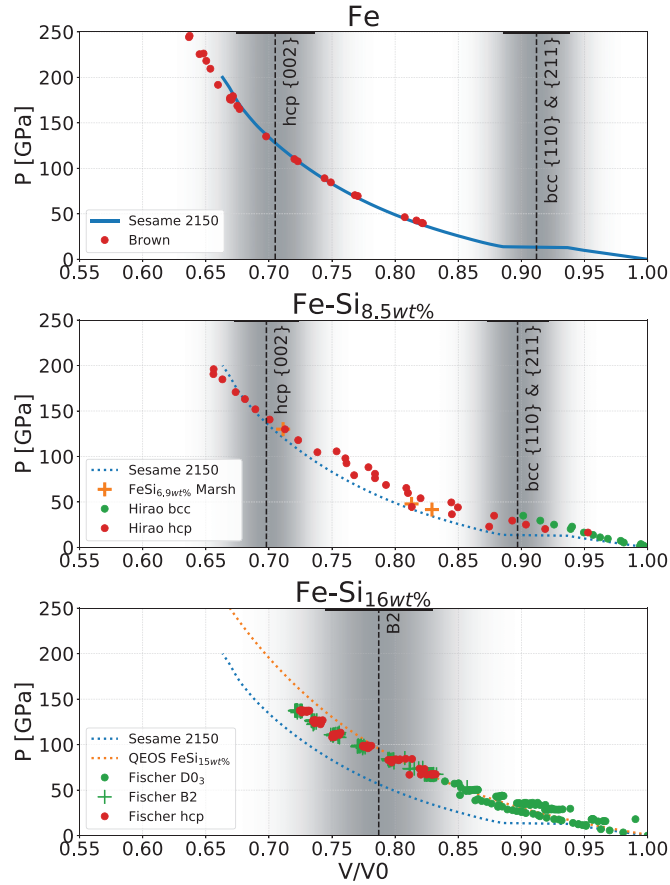

FIG. 4. Pressure-volume relations for Fe, Fe-$Si_{8.5\ wt\%}$, and Fe-$Si_{16\ wt\%}$. Black lines/gray shading show the volume and uncertainty of our measurements. In (a), the SESAME 2150 Hugoniot with data from Brown *et al.* [64]; (b) 300-K Fe-$Si_{8.7\ wt\%}$ static compression data [20] and Hugoniot data for Fe-$Si_{6.9\ wt\%}$ [63]; (c) static compression data for Fe-$Si_{16\ wt\%}$ [17] between 300 and 2200 K. (b) and (c) also show the SESAME 2150 Hugoniot.

Figure 5 shows DFT-predicted enthalpy versus pressure—the lowest enthalpy structure is considered thermodynamically stable. For Fe-$Si_{9.1\ wt\%}$, the ferromagnetic bcc phase dominates at low pressures, while hcp is most stable above ∼40 GPa. For Fe-$Si_{16.7\ wt\%}$, the ferromagnetic $D0_3$ phase dominates at low pressures. Starting at ∼60 GPa, the $B2$ phase stabilizes, with the hcp phase slightly less stable than $B2$ (by 20–50 meV/atom). The fcc phase remains metastable

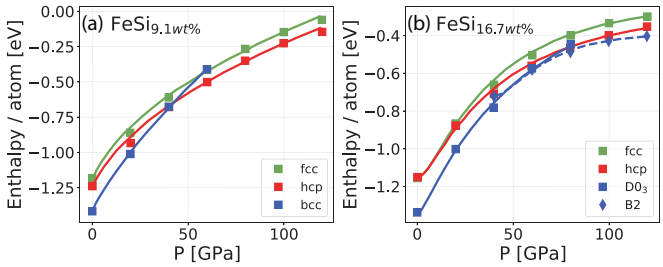

FIG. 5. Phase stability calculations using density functional theory at 0 K for (a) Fe-$Si_{9.1\ wt\,\%}$ and (b) Fe-$Si_{16.7\ wt\,\%}$.

at all pressures in both alloys. The increasing cubic phase stabilization for increasing Si concentration (Fig. 5) agrees with previous results [12,16–19] and our measurements on the point that small differences in Si concentration impact phase stability, in particular in the range ∼3–∼20 wt % of critical interest in planetary science.. This also highlights an advantage of using laser-driven compression, which is largely immune to diffusive concentration changes due to the timescale.

The different experimental timescales provide insight into the apparent inconsistencies across different reports. Our findings agree with Wicks *et al.* [18], suggesting that the process required to form the hcp phase observed by Fischer in Fe-$Si_{16\ wt\,\%}$ does not occur on the 1–10 ns timescale. DAC experiments typically occur on multisecond timescales enabling diffusive processes. While atomic rearrangement also occurs in dynamic compression due to plasticity, phase transformations, etc., bulk alloy concentration changes through diffusion are generally prohibited, though recent dynamic compression studies have revealed diffusive phase transformations active on tens of nanosecond timescales [33]. In our case, the rapid stabilization of the hcp structure for Fe and for Fe-$Si_{8.5\ wt\,\%}$, but not for Fe-$Si_{16\ wt\,\%}$, may imply that in this latter case the formation of the hcp phase requires nonmartensitic action such as diffusive demixing [68–73].

ACKNOWLEDGMENTS

The XFEL experiments were performed at the BL3 of SACLA with the approval of the Japan Synchrotron Radiation Research Institute (Proposals No. 2015A8023, No. 2015A8066, No. 2015B8014, No. 2015B8063, and No. 2017A8062). This work is in part supported by the French Agence Nationale de la Recherche with the ANR IRON-FEL 12-PDOC-0011, by the Japan Society for the Promotion of Science (JSPS) KAKENHI (Grants No. 16H01119 and No. 18H04368), JSPS core-to-core program on International Alliance for Material Science in Extreme States with High Power Laser and XFEL, the X-ray Free Electron Laser Priority Strategy Program at Osaka University from the Ministry of Education, Culture, Sports, Science, and Technology (Contract No. 12005014), the Centre National de la Recherche Scientifique GoToXFEL program, and under the auspices of the Lawrence Livermore National Security, LLC (LLNS) under Contract No. DE-AC52-07NA27344. This work was supported by the Department of Energy, Laboratory Directed Research and Development program at SLAC National Accelerator Laboratory, under Contract No. DE-AC02-76SF00515 and as part of the Panofsky Fellowship awarded to E.E.M. This work was further supported by Fusion Energy Sciences FWP10018. This project has also received funding from the European Research Council (ERC) under the European Union's Horizon 2020 research and innovation program (Grant Agreement No. 670787 D PLANETDIVE). D.A. has received funding from the European Research Council (ERC) under the European Union's Horizon 2020 research and innovation Programme (Grant Agreement No. 724690). We thank I. Estève for assistance with the scanning electron microscopy and B. Baptiste for assistance with the laboratory x-ray diffraction, that both allowed full characterization of the initial samples. We would like to thank A. Benuzzi-Mounaix, E. Edmund, G. Morard, and C. Wehrenberg for helpful discussions and A. Faenov, T. Pikuz, and Y. Tange for supporting the project.

[1] L. M. Barker and R. E. Hollenbach, J. Appl. Phys. **45**, 4872 (1974).

[2] D. H. Kalantar, J. F. Belak, G. W. Collins, J. D. Colvin, H. M. Davies, J. H. Eggert, T. C. Germann, J. Hawreliak, B. L. Holian, K. Kadau, P. S. Lomdahl, H. E. Lorenzana, M. A. Meyers, K. Rosolankova, M. S. Schneider, J. Sheppard, J. S. Stölken, and J. S. Wark, Phys. Rev. Lett. **95**, 075502 (2005).

[3] S. Tateno, K. Hirose, Y. Ohishi, and Y. Tatsumi, Science **330**, 359 (2010).

[4] A. E. Gleason and W. L. Mao, Nat. Geosci. **6**, 571 (2013).

[5] R. F. Smith, J. H. Eggert, D. C. Swift, J. Wang, T. S. Duffy, D. G. Braun, R. E. Rudd, D. B. Reisman, J.-P. Davis, M. D. Knudson, and G. W. Collins, J. Appl. Phys. **114**, 223507 (2013).

[6] R. G. Kraus, R. J. Hemley, S. J. Ali, J. L. Belof, L. X. Benedict, J. Bernier, D. Braun, R. E. Cohen, G. W. Collins, F. Coppari, M. P. Desjarlais, D. Fratanduono, S. Hamel, A. Krygier, A. Lazicki, J. Mcnaney, M. Millot, P. C. Myint, M. G. Newman, J. R. Rygg *et al.*, Science **375**, 202 (2022).

[7] V. Malavergne, P. Cordier, K. Righter, F. Brunet, B. Zanda, A. Addad, T. Smith, H. Bureau, S. Surblé, C. Raepsaet, E. Charon, and R. H. Hewins, Earth Planet. Sci. Lett. **394**, 186 (2014).

[8] N. L. Chabot, E. A. Wollack, R. L. Klima, and M. E. Minitti, Earth Planet. Sci. Lett. **390**, 199 (2014).

[9] R. Caracas and R. Wentzcovitch, Geophys. Res. Lett. **31**, L20603 (2004).

[10] D. Antonangeli, J. Siebert, J. Badro, D. L. Farber, G. Fiquet, G. Morard, and F. J. Ryerson, Earth Planet. Sci. Lett. **295**, 292 (2010).

[11] Z. Mao, J.-F. Lin, J. Liu, A. Alatas, L. Gao, J. Zhao, and H.-K. Mao, Proc. Natl. Acad. Sci. U.S.A. **109**, 10239 (2012).

[12] E. Edmund, G. Morard, M. A. Baron, A. Rivoldini, S. Boccato, K. Hirose, A. Pakhomova, and D. Antonangeli, Nat. Commun. **13**, 387 (2022).

[13] S. Yue, Y. Li, Q. Yang, K. Zhang, and C. Zhang, IEEE Trans. Magn. **55**, 1 (2019).

[14] E. Edmund, D. Antonangeli, F. Decremps, F. Miozzi, G. Morard, E. Boulard, A. Clark, S. Ayrinhac, M. Gauthier, M. Morand, and M. Mezouar, J. Geophys. Res.: Solid Earth **124**, 3436 (2019).

[15] I. Ohnuma, S. Abe, S. Shimenouchi, T. Omori, R. Kainuma, and K. Ishida, ISIJ Int. **52**, 540 (2012).

[16] R. A. Fischer, A. J. Campbell, R. Caracas, D. M. Reaman, P. Dera, and V. B. Prakapenka, Earth Planet. Sci. Lett. **357-358**, 268 (2012).

[17] R. A. Fischer, A. J. Campbell, D. M. Reaman, N. A. Miller, D. L. Heinz, P. Dera, and V. B. Prakapenka, Earth Planet. Sci. Lett. **373**, 54 (2013).

[18] J. K. Wicks, R. F. Smith, D. E. Fratanduono, F. Coppari, R. G. Kraus, M. G. Newman, J. R. Rygg, J. H. Eggert, and T. S. Duffy, Sci. Adv. **4**, eaao5864 (2018).

[19] E. Edmund, D. Antonangeli, F. Decremps, G. Morard, S. Ayrinhac, M. Gauthier, E. Boulard, M. Mezouar, M. Hanfland, and N. Guignot, Phys. Rev. B **100**, 134105 (2019).

[20] N. Hirao, E. Ohtani, T. Kondo, and T. Kikegawa, Phys. Chem. Miner. **31**, 329 (2004).

[21] R. A. Morrison, J. M. Jackson, W. Sturhahn, D. Zhang, and E. Greenberg, J. Geophys. Res.: Solid Earth **123**, 4647 (2018).

[22] E. Edmund, F. Miozzi, G. Morard, E. Boulard, A. Clark, F. Decremps, G. Garbarino, V. Svitlyk, M. Mezouar, and D. Antonangeli, Minerals **10**, 98 (2020).

[23] A. Belonoshko, N. Skorodumova, A. Rosengren, and B. Johansson, Science **319**, 797 (2008).

[24] C. M. Huntington, J. L. Belof, K. J. M. Blobaum, R. M. Cavallo, N. B. Kostinski, B. R. Maddox, H.-S. Park, C. Plechaty, S. T. Prisbrey, R. Rudd, D. W. Swift, R. J. Wallace, S. V. Weber, C. Wehrenberg, M. J. Wilson, and B. A. Remington, in *Shock Compression of Condensed Matter - 2015: Proceedings of the Conference of the American Physical Society Topical Group on Shock Compression of Condensed Matter*, AIP Conf. Proc. Vol. 1793 (AIP, Melville, NY, 2017), p. 110007

[25] A. Krygier, P. D. Powell, J. M. McNaney, C. M. Huntington, S. T. Prisbrey, B. A. Remington, R. E. Rudd, D. C. Swift, C. E. Wehrenberg, A. Arsenlis, H.-S. Park, P. Graham, E. Gumbrell, M. P. Hill, A. J. Comley, and S. D. Rothman, Phys. Rev. Lett. **123**, 205701 (2019).

[26] G. Morard, S. Boccato, A. D. Rosa, S. Anzellini, F. Miozzi, L. Henry, G. Garbarino, M. Mezouar, M. Harmand, F. Guyot, E. Boulard, I. Kantor, T. Irifune, and R. Torchio, Geophys. Res. Lett. **45**, 11,074 (2018).

[27] S. Merkel, N. Miyajima, D. Antonangeli, G. Fiquet, and T. Yagi, J. Appl. Phys. **100**, 023510 (2006).

[28] R. G. Kraus, J.-P. Davis, C. T. Seagle, D. E. Fratanduono, D. C. Swift, J. L. Brown, and J. H. Eggert, Phys. Rev. B **93**, 134105 (2016).

[29] A. Dewaele, A. B. Belonoshko, G. Garbarino, F. Occelli, P. Bouvier, M. Hanfland, and M. Mezouar, Phys. Rev. B **85**, 214105 (2012).

[30] H. Okamoto, J. Phase Equilib. **13**, 543 (1992).

[31] J. Verhoogen, Philos. Trans. R. Soc. London, Ser. A **258**, 276 (1965).

[32] J. R. Rygg, R. F. Smith, A. E. Lazicki, D. G. Braun, D. E. Fratanduono, R. G. Kraus, J. M. McNaney, D. C. Swift, C. E. Wehrenberg, F. Coppari, M. F. Ahmed, M. A. Barrios, K. J. M. Blobaum, G. W. Collins, A. L. Cook, P. D. Nicola, E. G. Dzenitis, S. Gonzales, B. F. Heidl, M. Hohenberger *et al.*, Rev. Sci. Instrum. **91**, 043902 (2020).

[33] A. E. Gleason, C. A. Bolme, H. J. Lee, B. Nagler, E. Galtier, D. Milathianaki, J. Hawreliak, R. G. Kraus, J. H. Eggert, D. E. Fratanduono, G. W. Collins, R. Sandberg, W. Yang, and W. L. Mao, Nat. Commun. **6**, 8191 (2015).

[34] B. Albertazzi, N. Ozaki, V. Zhakhovsky, A. Faenov, H. Habara, M. Harmand, N. Hartley, D. Ilnitsky, N. Inogamov, Y. Inubushi, T. Ishikawa, T. Katayama, T. Koyama, M. Koenig, A. Krygier, T. Matsuoka, S. Matsuyama, E. McBride, K. P. Migdal, G. Morard *et al.*, Sci. Adv. **3**, e1602705 (2017).

[35] N. J. Hartley, N. Ozaki, T. Matsuoka, B. Albertazzi, A. Faenov, Y. Fujimoto, H. Habara, M. Harmand, Y. Inubushi, T. Katayama, M. Koenig, A. Krygier, P. Mabey, Y. Matsumura, S. Matsuyama, E. E. McBride, K. Miyanishi, G. Morard, T. Okuchi, T. Pikuz *et al.*, Appl. Phys. Lett. **110**, 071905 (2017).

[36] E. E. McBride, A. Krygier, A. Ehnes, E. Galtier, M. Harmand, Z. Konôpková, H. J. Lee, H.-P. Liermann, B. Nagler, A. Pelka, M. Rödel, A. Schropp, R. F. Smith, C. Spindloe, D. Swift, F. Tavella, S. Toleikis, T. Tschentscher, J. S. Wark, and A. Higginbotham, Nat. Phys. **15**, 89 (2019).

[37] A. L. Coleman, M. G. Gorman, R. Briggs, R. S. McWilliams, D. McGonegle, C. A. Bolme, A. E. Gleason, D. E. Fratanduono, R. F. Smith, E. Galtier, H. J. Lee, B. Nagler, E. Granados, G. W. Collins, J. H. Eggert, J. S. Wark, and M. I. McMahon, Phys. Rev. Lett. **122**, 255704 (2019).

[38] M. J. MacDonald, E. E. McBride, E. Galtier, M. Gauthier, E. Granados, D. Kraus, A. Krygier, A. L. Levitan, A. J. MacKinnon, I. Nam, W. Schumaker, P. Sun, T. B. van Driel, J. Vorberger, Z. Xing, R. P. Drake, S. H. Glenzer, and L. B. Fletcher, Appl. Phys. Lett. **116**, 234104 (2020).

[39] C. E. Wehrenberg, D. McGonegle, C. Bolme, A. Higginbotham, A. Lazicki, H. J. Lee, B. Nagler, H.-S. Park, B. A. Remington, R. E. Rudd, M. Sliwa, M. Suggit, D. Swift, F. Tavella, L. Zepeda-Ruiz, and J. S. Wark, Nature (London) **550**, 496 (2017).

[40] B. J. Jensen, G. T. Gray, and R. S. Hixson, J. Appl. Phys. **105**, 103502 (2009).

[41] N. Amadou, T. de Resseguier, E. Brambrink, T. Vinci, A. Benuzzi-Mounaix, G. Huser, G. Morard, F. Guyot, K. Miyanishi, N. Ozaki, R. Kodama, and M. Koenig, Phys. Rev. B **93**, 214108 (2016).

[42] C. Langrand, D. Andrault, S. Durand, Z. Konôpková, N. Hilairet, C. Thomas, and S. Merkel, Nat. Commun. **10**, 5680 (2019).

[43] T. Ishikawa, H. Aoyagi, T. Asaka, Y. Asano, N. Azumi, T. Bizen, H. Ego, K. Fukami, T. Fukui, Y. Furukawa, S. Goto, H. Hanaki, T. Hara, T. Hasegawa, T. Hatsui, A. Higashiya, T. Hirono, N. Hosoda, M. Ishii, T. Inagaki *et al.*, Nat. Photonics **6**, 540 (2012).

[44] K. Tono, Y. Inubushi, M. Yabashi, H. Tanaka, K. Tiedtke, and A. Azima, New J. Phys. **15**, 083035 (2013).

[45] Y. Inubushi, T. Yabuuchi, T. Togashi, K. Sueda, K. Miyanishi, Y. Tange, N. Ozaki, T. Matsuoka, R. Kodama, T. Osaka, S. Matsuyama, K. Yamauchi, H. Yumoto, T. Koyama, H. Ohashi, K. Tono, and M. Yabashi, Appl. Sci. **10**, 2224 (2020).

[46] A. Dewaele, C. Denoual, S. Anzellini, F. Occelli, M. Mezouar, P. Cordier, S. Merkel, M. Véron, and E. Rausch, Phys. Rev. B **91**, 174105 (2015).

[47] See Supplemental Material at http://link.aps.org/supplemental/10.1103/PhysRevB.105.L220102 for additional experimental

details, radiation hydrodynamics simulations, and density functional theory calculations.

[48] J. W. Swegle and D. E. Grady, J. Appl. Phys. **58**, 692 (1985).

[49] D. Errandonea, D. Santamaría-Perez, A. Vegas, J. Nuss, M. Jansen, P. Rodríguez-Hernandez, and A. Muñoz, Phys. Rev. B **77**, 094113 (2008).

[50] D. Santamaría-Perez, D. Errandonea, A. Vegas, J. Nuss, M. Jansen, P. Rodríguez-Hernández, A. Muñoz, and R. Boehler, J. Phys.: Conf. Ser. **121**, 022013 (2008).

[51] S. Malviya, R. R. Kinge, N. Kaurav, and R. C. Dixit, in *National Conference on Physics and Chemistry of Materials (NCPCM 2020)*, edited by N. Kaurav, K. K. Choudhary, R. C. Dixit, and G. D. Gupta, AIP Conf. Proc. Vol. 2369 (AIP, Melville, NY, 2021), p. 020133.

[52] K. Kadau, T. C. Germann, P. S. Lomdahl, and B. L. Holian, Science **296**, 1681 (2002).

[53] K. Kadau, T. C. Germann, P. S. Lomdahl, and B. L. Holian, Phys. Rev. B **72**, 064120 (2005).

[54] K. Kadau, T. C. Germann, P. S. Lomdahl, R. C. Albers, J. S. Wark, A. Higginbotham, and B. L. Holian, Phys. Rev. Lett. **98**, 135701 (2007).

[55] H. Hwang, E. Galtier, H. Cynn, I. Eom, S. H. Chun, Y. Bang, G. C. Hwang, J. Choi, T. Kim, M. Kong, S. Kwon, K. Kang, H. J. Lee, C. Park, J. I. Lee, Y. Lee, W. Yang, S. H. Shim, T. Vogt, S. Kim *et al.*, Sci. Adv. **6**, eaaz5132 (2020).

[56] D. McGonegle, D. Milathianaki, B. A. Remington, J. S. Wark, and A. Higginbotham, J. Appl. Phys. **118**, 065902 (2015).

[57] D. N. Polsin, D. E. Fratanduono, J. R. Rygg, A. Lazicki, R. F. Smith, J. H. Eggert, M. C. Gregor, B. H. Henderson, J. A. Delettrez, R. G. Kraus, P. M. Celliers, F. Coppari, D. C. Swift, C. A. McCoy, C. T. Seagle, J.-P. Davis, S. J. Burns, G. W. Collins, and T. R. Boehly, Phys. Rev. Lett. **119**, 175702 (2017).

[58] J. A. Hawreliak, B. El-Dasher, H. Lorenzana, G. Kimminau, A. Higginbotham, B. Nagler, S. M. Vinko, W. J. Murphy, T. Whitcher, J. S. Wark, S. Rothman, and N. Park, Phys. Rev. B **83**, 144114 (2011).

[59] R. A. Fischer and A. J. Campbell, Am. Mineral. **100**, 2718 (2015).

[60] J. H. Woodhouse, D. Giardini, and X.-D. Li, Geophys. Res. Lett. **13**, 1549 (1986).

[61] A. Morelli, A. M. Dziewonski, and J. H. Woodhouse, Geophys. Res. Lett. **13**, 1545 (1986).

[62] D. Antonangeli, S. Merkel, and D. L. Farber, Geophys. Res. Lett. **33**, L24303 (2006).

[63] S. P. Marsh, *LASL Shock Hugoniot Data*, Vol. 5 (University of California Press, Berkeley, CA, 1980).

[64] J. M. Brown, J. N. Fritz, and R. S. Hixson, J. Appl. Phys. **88**, 5496 (2000).

[65] J. P. Perdew, K. Burke, and M. Ernzerhof, Phys. Rev. Lett. **77**, 3865 (1996).

[66] C. J. Pickard and R. J. Needs, J. Phys.: Condens. Matter **23**, 053201 (2011).

[67] G. Mogni (private communication).

[68] X. Daura, K. Gademann, B. Jaun, D. Seebach, W. F. van Gunsteren, and A. E. Mark, Angew. Chem., Int. Ed. **38**, 236 (1999).

[69] G. A. Gallet and F. Pietrucci, J. Chem. Phys. **139**, 074101 (2013).

[70] H. K. Mao, Y. Wu, L. C. Chen, J. F. Shu, and A. P. Jephcoat, J. Geophys. Res. **95**, 21737 (1990).

[71] P. Giannozzi, S. Baroni, N. Bonini, M. Calandra, R. Car, C. Cavazzoni, D. Ceresoli, G. L. Chiarotti, M. Cococcioni, I. Dabo, A. D. Corso, S. de Gironcoli, S. Fabris, G. Fratesi, R. Gebauer, U. Gerstmann, C. Gougoussis, A. Kokalj, M. Lazzeri, L. Martin-Samos *et al.*, J. Phys.: Condens. Matter **21**, 395502 (2009).

[72] P. Giannozzi, O. Andreussi, T. Brumme, O. Bunau, M. B. Nardelli, M. Calandra, R. Car, C. Cavazzoni, D. Ceresoli, M. Cococcioni, N. Colonna, I. Carnimeo, A. D. Corso, S. de Gironcoli, P. Delugas, R. A. DiStasio, A. Ferretti, A. Floris, G. Fratesi, G. Fugallo *et al.*, J. Phys.: Condens. Matter **29**, 465901 (2017).

[73] R. M. More, K. H. Warren, D. A. Young, and G. B. Zimmerman, Phys. Fluids **31**, 3059 (1988).